Chemical Vapor Deposition of Mercury on Alkanedithiolate Self-Assembled Monolayers

Anne Kathrena A. Aliganga,[†] Zhehui Wang,[‡] and Silvia Mittler*[†,§]

Max Planck Institute for Polymer Research, Ackermannweg 10, D-55128 Mainz, Germany, Institute of Physical Chemistry, Technical University of Clausthal, Arnold-Sommerfeld-Str. 4, D-38678 Clausthal Zellerfeld, Germany, and Department of Physics and Astronomy, The University of Western Ontario, London, Ontario N6A 3K7, Canada

Received: December 11, 2003

This paper describes the selective deposition of mercury (Hg) onto self-assembled dithiols via a chemical vapor deposition (CVD) process. Characterizations of the deposited Hg by atomic force microscopy (AFM) after its chemisorption with the -thiol head groups showed particle-like behavior. The AFM results obtained posed an interesting question regarding the physical state of the deposited Hg: are nanodroplets or nanoparticles formed? The determination of the nanosized-droplets formation of Hg on alkanedithiolate self-assembled monolayers (SAMs) is demonstrated using quartz crystal microbalance (QCM) technique.

Introduction

Mercury has been the subject of several electron-transfer studies.[1,2] Electron-transfer steps play an important role in many homogeneous and heterogeneous reactions.[3,4] In this process, a large barrier for the electron transfer between donor and acceptor may occur, which might restrict the passage of an electron. An effective catalyst, with an intermediate redox potential value of the donor−acceptor pair, helps the transfer of electrons from donor to acceptor and acts as an electron relay system.[5−9] Metal ions or metal particles are well-known examples of this type of redox catalyst. Jana et al.[1] have successfully demonstrated the redox catalytic properties of small mercury particles using methylene blue as a redox probe. They showed the possibility of electron transfer from the reducing agent to the dye via the Hg nanoparticles, which act as electron-transfer catalyst.

Another important use of Hg is to aid in understanding the flow of electrons through organic matter. This is important in several areas, such as the rationalization of electron transfer in biological molecules, the fabrication of microelectronic devices and sensors, and the development of molecular electronics. In these aspects Hg has been commonly used as a metal support[10−14] or as an electrode.[15,16] Mercury offers several advantages in comparison to other metals. First, it allows to readily form self-assembled monolayers of alkanethiols that have been characterized structurally. Second, it is a liquid at room temperature. A liquid Hg surface supporting a SAM is compliant and can conform to the topography of a solid surface with which it is brought into contact. This ability to conform minimizes the effects of irregularities of the solid surface on the structure of the SAMs. This further provides the SAMs with better passivating properties (a much smaller number of defects) and stability making them suitable candidates for use in nano- and molecular-scale electronic devices.

Regardless of the physical state of Hg, whether it is in the form of nanosized particles or a liquid droplet, Hg has proven to play an important role in the vast field of research. In this paper, the deposition of Hg on alkanedithiolate SAMs under ambient laboratory conditions and the determination of the physical state of the deposited Hg are presented.

The formation of SAMs of thiols on different metal surface such as gold, silver, and mercury is still subject to controversy even though numerous studies covering the understanding of the preparation, properties, and structure of these densely-packed and well-ordered SAMs have been reported.[17−26] The thiol-metal bond is most commonly described as a surface-bound thiolate and the sulfur-bound hydrogen is generally assumed to be absent in these systems. Several mechanisms have been proposed for thiol adsorption on different metal surfaces.[27−29] A combination of both scenarios in which hydrogen is still bound to the sulfur and adsorbed on the metal surface appears to be taking place.[28] Most likely, the desorption of molecular hydrogen via adsorbed atomic hydrogen is a feasible mechanism of hydrogen loss in these systems as well as in SAMs on a macroscopic surface. This is supported by experiments done recently.[30,31] While the nature of thiol-metal bonds and the structural properties of the resulting SAMs are still matters of an intense current research effort, the focus of several activities is the deposition of inorganic materials on the surface of SAMs.[32−37] The focus is the same in this work; 1,8-octanedithiol (C8-DT) SAMs have been used as the reactive head groups for the nucleation and growth of CVD Hg.

Hg nanoparticles are usually prepared via solution chemistry by the reduction of an Hg_2Cl_2 solution with $NaBH_4$. In this work, preparation of Hg on SAMs was done at ambient conditions very similar to the very mild conditioned organometallic chemical vapor deposition experiments (OMCVD) of gold and other materials performed by our group recently.[32−34,38] In these studies we have not only proven the possibility of growing various materials and gold nanoparticles on template SAMs, but also that no mixing with the underlying metal occurs, as well as the influence on diluting the nucleation sites. Grunze et al.[39] has employed a similar sample preparation for mercury. The main difference was that Grunze et al.[39] used alkanethiolate SAMs since their study focused on the changes in molecular structure of methyl-terminated alkanethiolate SAMs on polycrystalline gold induced by exposure to Hg vapor. They found an increase in lateral chain density in SAMs of alkanethiols on Au after exposure of the alkanethiolate monolayers to Hg vapor

* To whom correspondence should be addressed. E-mail: smittler@uwo.ca; Phone: ++ 1 (519) 661-2111 loc. 88592; Fax: ++ 1 (519) 661-2033.
[†] Max Planck Institute for Polymer Research.
[‡] Institute of Physical Chemistry, Technical University of Clausthal.
[§] Department of Physics and Astronomy, The University of Western Ontario.

10.1021/jp031315e CCC: $27.50
Published on Web 07/02/2004

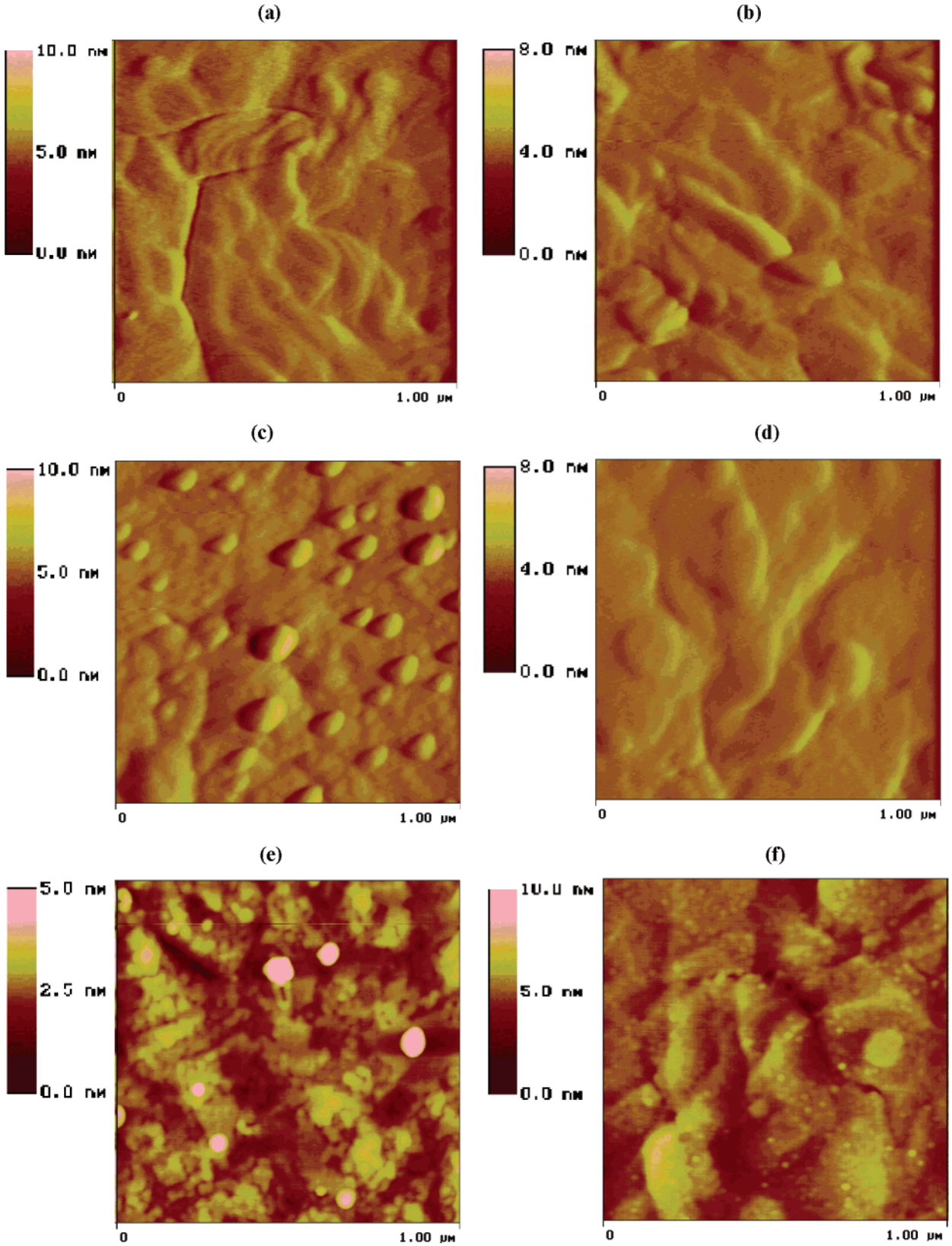

Figure 1. AFM images of SAMs of (a) 1,8-octanedithiol (C8-DT) and (b) 1-octanethiol (C8-T) on Au (111). CVD Hg on SAMs of (c) C8-DT and (d) C8-T after 20 min, and CVD Hg on SAMs of (e) C8-DT and (f) C8-T after 24 h reaction times.

and a subsequent reimmersion into the thiol solution. In this work, however, the growth and phase of Hg nanoobjects on alkanedithiolate SAMs are given emphasis after the Hg chemisorbed with the exposed thiol head groups. SAMs of alkanethiolate and −dithiolate on an atomically-flat Au (111) surface were used as a substrate and growth/nongrowth templates for Hg nanoobject growth. The deposited Hg onto the SAMs was first characterized using AFM techniques and its liquid−solid phase transition was monitored by a Quartz Crystal Microbalance (QCM).

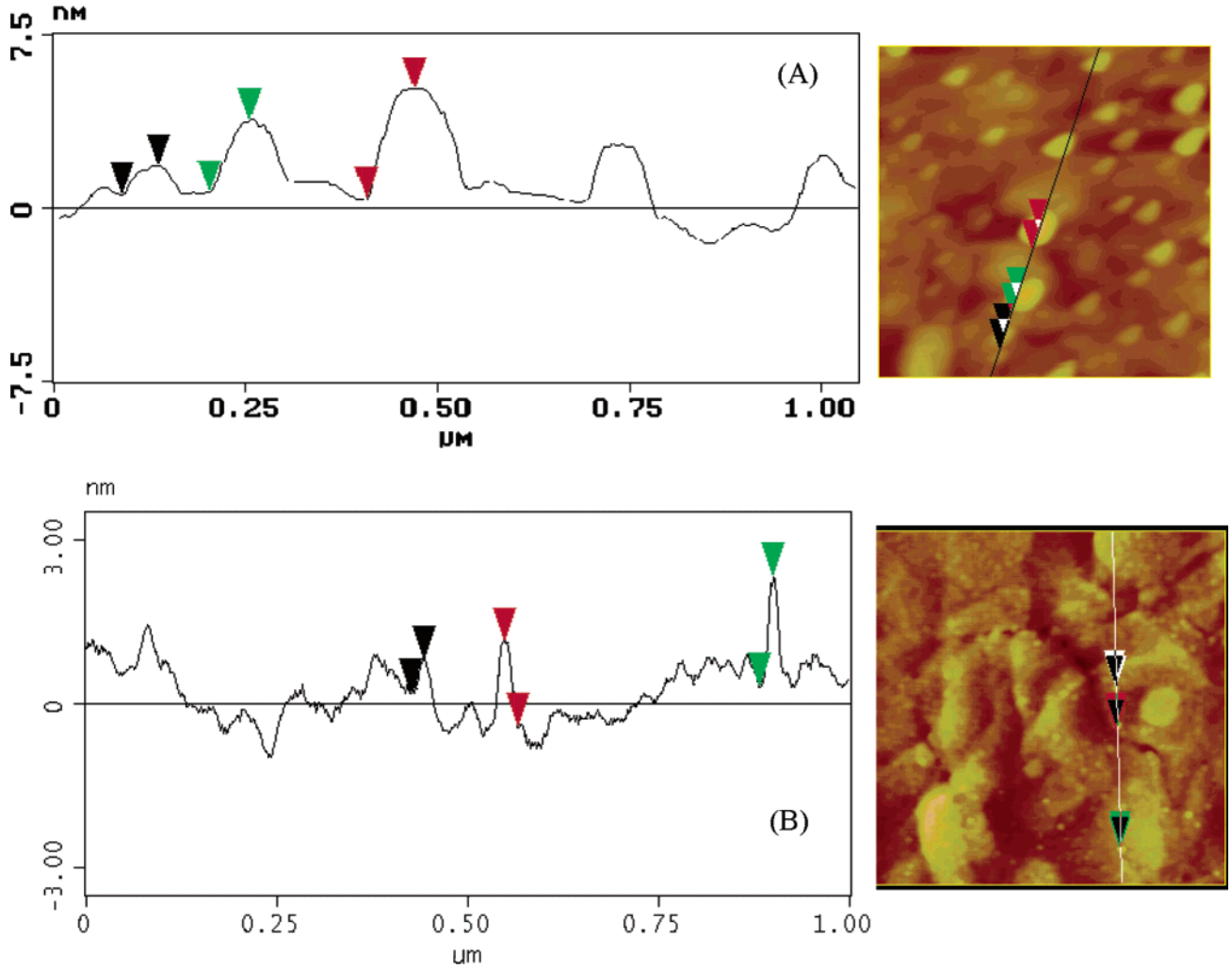

Figure 2. Section analysis of the flattened AFM image of (a) CVD Hg on C8-DT after 20 min reaction time, and (b) CVD Hg on C8-T after 24 h reaction time.

Experimental Section

A. Au(111) Preparation. Gold (Balzers, 99.99%) was deposited onto freshly-cleaved mica substrates using a vacuum coating system (Edwards, FL 400) at $p \leq 5 \times 10^{-6}$ mbar. Before deposition, the mica was heated to 650 °C for 3−4 min under a N_2 atmosphere. It was immediately placed inside the vacuum evaporation machine. The typical evaporation rate was 1 Å/s, and the thickness of gold film was 60 nm. Prior to the self-assembly process, these freshly-evaporated Au-on-mica samples were annealed to form large areas with (111) orientations on the surface. Annealing was carried out at 650 °C for 1 min under a N_2 atmosphere in a tubular oven (Heraeus) and the samples were chilled to room temperature under a N_2 atmosphere. This method produced flat Au (111) terraces as large as 300 nm × 300 nm based from our AFM measurements.

B. SAM Preparation. 1-Octanethiol (C8-T; Aldrich, 98.5+ %), 1,8-octanedithiol (C8-DT; Aldrich, 97+ %) and ethanol (Chromasolv, Riedel-de Haën) were used without further purification. SAMs were prepared by immersing freshly-prepared Au in a 1 mM ethanolic solution of the respective alkanethiol or −dithiol for approximately 12 h. The samples were then cleaned by rinsing extensively with ethanol, dried with N_2, and stored under inert conditions (sealed in a glass flask under an Ar atmosphere).

C. Deposition of Hg on SAMs of 1-Octanethiol and 1,8-Octanedithiol. A drop of pure Hg was placed inside a small capped Petri dish and allowed to stand at room temperature for 30 min for saturation with mercury vapor. The SAM was then added to the Petri dish and capped again. The SAMs were exposed to the saturated Hg vapor at room temperature for a period of time ranging from 20 min to 2 days. At room temperature (25 °C) the saturation vapor pressure of Hg in air is 0.0017 mbar (0.170 Pa). This corresponds to a mercury vapor concentration of 13.6 mg/m^3 of air.[40]

D. Atomic Force Microscopy (AFM). AFM images were acquired using a Nanoscope IIIa Atomic Force Microscope (Digital Instruments, Santa Barbara, CA). Imaging was done in contact and tapping mode at ambient conditions. Silicon nitride cantilevers of 100 μm length (spring constant 0.1 N/m) with integrated sharpened tips (Olympus, Tokyo, Japan) were used.

E. Quartz Crystal Microbalance (QCM). For QCM analysis of the adsorbed mercury, deposition experiments were carried out on the front electrode of a quartz crystal microbalance. The overtone-polished, gold-coated AT-cut quartz crystals (Maxtek, Torrance, CA) had an outer diameter of 1 inch. The self-assembled monolayer was deposited on the front electrode of the quartz plate in the usual way. The quartz plate was connected to an impedance analyzer (E5100A, Agilent). Resonance frequency and bandwidth were determined by fitting resonance curves to the conductance spectra as described previously.[41]

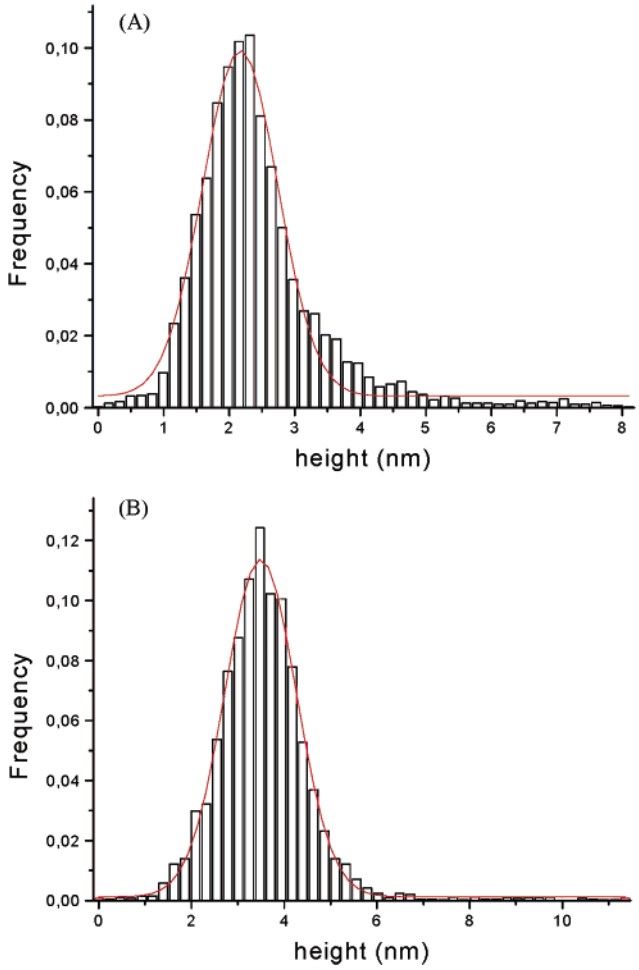

Figure 3. Height distribution of the Hg nanoobjects on C8-DT SAMs after (a) 20 min and after (b) 48 h.

Results and Discussion

1. Particle-Like Behavior of Hg on SAMs by AFM. AFM analysis was performed to determine the surface morphology of the deposited Hg on SAMs. Figure 1 shows a gallery of AFM images of Hg on SAMs at different reaction times. A relatively-flat surface is shown in Figure 1a (dithiol) and 1b (thiol) with only the SAM on the surface. The terraces of Au (111) on mica measuring around 200−300 nm are clearly observed. Exposure of 1,8-octanedithiolate SAMs to Hg vapor for 20 min provides particle-like morphologies on the surface (Figure 1c). The structures have elongated spherical shapes independent of the scanning direction, with heights ranging from 1 to 5 nm (Figure 2a). They are not moved around or smeared out by the contact mode scanning modus. To further confirm the selectivity of the CVD process on thiol surfaces only as reported previously,[32,33] a parallel deposition run of Hg on 1-octanethiol with CH_3 head groups was performed for 20 min. There were no particle-like structures found (Figure 1d) compared to the structures observed in Figure 1c. However, increasing the deposition times of Hg to 2 days gave well-packed aggregates of particle-like structures for the dithiol head groups sample (Figure 1e), whereas, spherical particle-like structures with heights ranging from 6 Å to 2 nm (Figure 2b) were obtained for the CH_3 head group sample (Figure 1f). The particle height distribution for the growth-template C8-DT was investigated for the 20 min and the 48 h samples (Figure 3a and b). The lines are fits to a Gaussian profile. The mean particle height of 2 nm increases with increasing deposition time to 3.5 nm. The distribution width

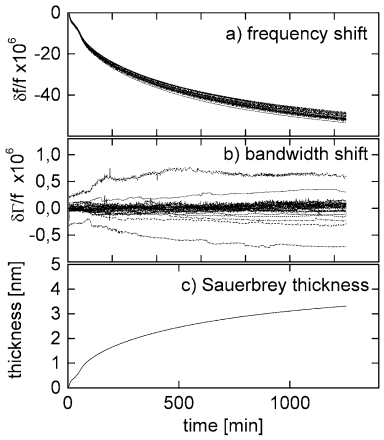

Figure 4. Deposition of Hg on SAMs as monitored by QCM at 25 °C for 21 h. (a) Fractional frequency shifts $\delta f/f$ and (b) bandwidth shift $\delta\Gamma/f$ versus time. (c) Film thickness of the deposited Hg as derived from the frequency shift by the Sauerbrey equation.[44]

is not affected seriously. Similar results have been obtained with the OMCVD of gold nanoparticles on this C8-DT using the $(CH_3)_3PAuCH_3$ -precursor. In this case it was also possible to measure the width distribution by electron microscopy.[42] Because of contamination concerns this cannot be done with mercury.

At this point, it would have been tempting to say that nanoparticles of Hg were deposited on the surface wherein Hg is covalently bonded to the present SH-groups as we have observed for various other OMCVD-deposited materials. Otherwise, the structures would have been removed or destroyed after several scans with the AFM needle on the surface, especially using the contact mode. However, the high surface tension of Hg, which keeps the nanostructures intact on the surface while scanning with the AFM needle, could not be ignored in this case. The interfacial tension of Hg and air is 485.48×10^{-3} N/m at laboratory conditions, which is approximately 7 times higher than the surface tension of water (71.99×10^{-3} N/m) and 10 times larger than that of common liquids.[43] This was affirmed by using the tapping mode in AFM imaging, which yielded very similar images to the contact mode and gave no evidence for either the liquid or the solid state of the objects also taking the phase images into account.

From the AFM results of the CVD Hg on SAMs of 1-octanethiol and 1,8-octanedithiol, it is difficult to distinguish whether Hg nanoparticles or nanodroplets were formed by the deposition of Hg on the surface. In this regard, QCM experiments were employed to reveal the state of Hg on SAMs.

2. Liquid−Solid-Phase Transition Determination of Mercury on SAMs as Monitored by QCM. Data were taken on many overtones in parallel in order to investigate possible effects of viscoelasticity. Figure 4 shows the results of an online deposition experiment of Hg on a C8-DT SAM located on the quartz crystal microbalance (QCM). Panels (a) and (b) display the fractional frequency shift $\delta f/f$ and the shift in bandwidth $\delta\Gamma$. Panel (c) shows the film thickness as derived from the frequency shift by the Sauerbrey equation[44]

$$t_f = \frac{1}{\rho_f}\frac{Z_q}{2f_o}\frac{\delta f}{f} \qquad (1)$$

where t_f is the film thickness, $\rho_f = 13.53359$[41] is the density of mercury, $Z_q = 8.8 \cdot 10^6$ is the acoustic impedance of AT-cut quartz, and $f_o = 5$ MHz is the frequency of the fundamental.

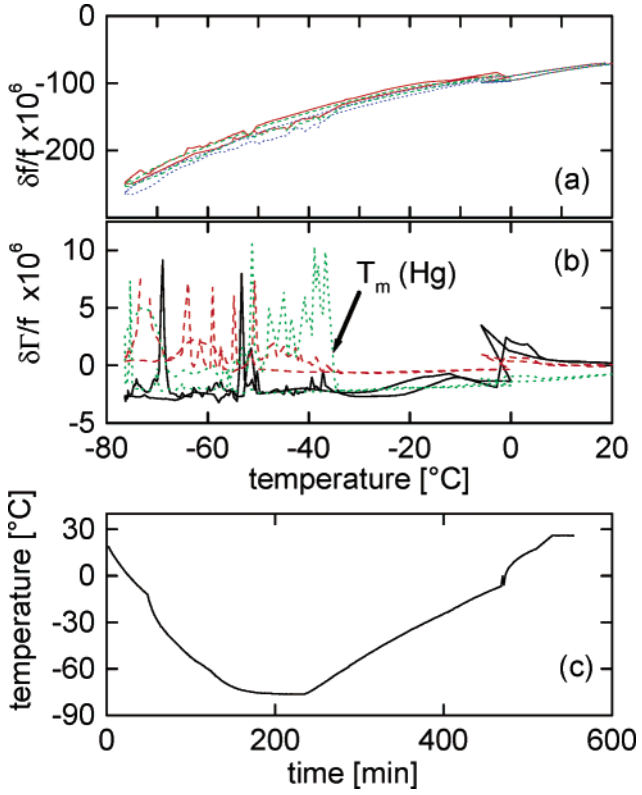

Figure 5. QCM temperature sweep of Hg on a SAM of 1,8-octanedithiol on an Au-coated quartz surface. (a) fractional frequency shifts and (b) bandwidth in various harmonics. (c) Temperature program versus time.

The fractional frequency $\delta f/f$ shift is virtually the same on all harmonics. The shift in bandwidth is comparable to the noise level. From these two findings one concludes that viscoelastic effects are absent. While one might be tempted to interpret this result in the sense that the deposited film is a solid, the detailed calculation shows that the experimental data are also compatible with a liquid film. Viscoelastic effects scale as the third power of film thickness and become very small for thin films. At a thickness of 3 nm, the distinction between a liquid and a solid film cannot be based on the QCM data alone.

To obtain further insight into the state of the adsorbate, we have performed a cooling experiment on the Hg nanoobjects located on a C8-DT SAM on the quartz crystal in order to detect a possible phase transition between the liquid and the solid state. After Hg naonoobject deposition the sample was slowly cooled to −70 °C and heated back up to room temperature. Figure 5 shows these QCM data. The frequency shift is entirely dominated by temperature-frequency coupling. The bandwidth reveals a clear signature at −34 °C, which agrees with the literature value of the melting point (−39 °C) within the experimental error. The bandwidth *increases* below the melting point. Presumably, the increase is caused by internal stress related to the crystallization. Regardless of the detailed explanation one clearly observes a phase transition. Based on the temperature where the transition occurs, the phase transition can be assigned to freezing. This necessarily implies that the deposited mercury film is in the liquid state.

Conclusions

Deposition of Hg on template SAMs of 1,8-octanedithiol under ambient laboratory conditions was successfully demonstrated for a 20 min deposition time. Long deposition times such as 48 h ead to a growth of Hg nanodroplets both on growth and nongrowth surfaces. The state of the deposited Hg was not primarily determined with AFM because the high surface tension of Hg keeps the droplets undistorted by the scanning with the AFM needle both in contact and tapping mode. With the QCM phase transition experiment, the deposited Hg was found to be in the liquid state and have the same phase transition temperature as bulk mercury.

Acknowledgment. The authors thank Diethelm Johannsmann for the valuable comments and discussions, especially on the QCM results, and the BMBF and its Center for Multifunctional Materials, as well as the DFG for kind financial support.

References and Notes

(1) Jana, N. R.; Pal, T. *Indian J. Chem.* **2001**, *40A*, 403.
(2) Buoninsegni, F. T.; Herrero, R.; Moncelli, M. R. *J. Electroanal. Chem.* **1998**, *452*, 33.
(3) Wilkinson, G. Gillard, R. D.; McCleverty, J. A.; *Comprehensive Coordination Chemistry*; Pergamon Press: Oxford, 1987; Vol. 1.
(4) Compton, R. G. *Comprehensive Chemical Kinetics*; Elsevier: New York, 1989; Vol. 28.
(5) Zaera, F.; Gellman, A. J.; Somorjai, G. A. *Acc. Chem. Res.* **1986**, *19*, 24.
(6) Hercules, D. M.; Proctor, A.; Houlla, M. *Acc. Chem. Res.* **1994**, *27*, 387.
(7) Sun, T.; Seff, K. *Chem. Rev.* **1994**, *94*, 857.
(8) Schmid, G. *Chem. Rev.* **1992**, *92*, 1709.
(9) Lewis, L. N. *Chem. Rev.* **1993**, *93*, 2693.
(10) Holmlin, R. E.; Haag, R.; Chabinye, M. L.; Ismagilov, R. F.; Cohen, A. E.; Terfort, A.; Rampi, M. A.; Whitesides, G. M. *J. Am. Chem. Soc.* **2001**, *123*, 5075.
(11) Rampi, M. A.; Schueller, O. J. A.; Whitesides, G. M. *Appl. Phys. Lett.* **1998**, *72*, 1781.
(12) Holmlin, R. E.; Haag, R.; Ismagilov, R. F.; Cohen, A. E.; Terfort, A.; Rampi, M. A.; Whitesides, G. M. *Book of Abstracts, 218th ACS National Meeting*; New Orleans, 1999.
(13) Haag, R.; Rampi, M. A.; Whitesides, G. M. *Book of Abstracts, 216th ACS National Meeting*; Boston, 1998.
(14) Buoninsegni, F. T.; Herrero, R.; Moncelli, M. R. *J. Electroanal. Chem.* **1998**, *452*, 33.
(15) Haag, R.; Rampi, M. A.; Holmlin, R. E.; Whitesides, G. M. *J. Am. Chem. Soc.* **1999**, *121*, 7895.
(16) Krysinski, P.; Moncelli, M. R.; Tadini-Buoninsegni, F. *Electrochim. Acta* **2000**, *45*, 1885.
(17) Porter, M. D.; Bright, T. B.; Allara, D. L.; Chidsey, C. E. D. *J. Am. Chem. Soc.* **1987**, *109*, 3559.
(18) Strong, L.; Whitesides, G. M. *Langmuir* **1988**, *4*, 546.
(19) Kim, Y. T.; Bard, A. J. *Langmuir* **1992**, *8*, 1096.
(20) Pan, J.; Tao N.; Lindsay, S. M. *Langmuir* **1993**, *9*, 1556.
(21) Laibinis, P. E.; Whitesides, G. M.; Allara, D. L.; Tao, Y.-T.; Parikh, A. N.; Nuzzo, R. G. *J. Am. Chem. Soc.* **1991**, *113*, 7152.
(22) Zhong, C. J.; Porter, M. D. *J. Electroanal. Chem.* **1997**, *425*, 147.
(23) Jung, C. H.; Dannenberger, O.; Xu, Y.; Buck, M.; Grunze, M. *Langmuir* **1998**, *14*, 1103.
(24) Himmelhaus, M.; Eisert, F.; Buck, M.; Grunze, M. *J. Phys. Chem. B* **2000**, *104*, 576.
(25) Muskal, N.; Mandler, D. *Electrochim. Acta* **1999**, *45*, 537.
(26) Schreiber, F. *Prog. Surf. Sci.* **2000**, *65*, 151.
(27) Nuzzo, R. G.; Zegarski, B. R.; Dubois, L. H.; *J. Am. Chem. Soc.* **1987**, *109*, 733.
(28) Grönbeck, H.; Curioni, A.; Andreoni, W. *J. Am. Chem. Soc.* **2000**, *122*, 3839.
(29) Hostetler, M. J.; Templeton, A. C.; Murray, R. W. *Langmuir* **1999**, *15*, 3782.
(30) Hasan, M.; Bethell, D.; Brust, M. *J. Am. Chem. Soc.* **2002**, *124*, 1132.
(31) Cohen-Atiya, M.; Mandler, D. *J. Electroanal. Chem.* **2003**, *550−551*, 267.
(32) Wohlfart, P.; Weiss, J.; Käshammer, J.; Winter, C.; Scheumann, V.; Fischer, R. A.; Mittler-Neher, S. *Thin Solid Films* **1999**, *340*, 274.
(33) Winter, C.; Weckenmann, U.; Fischer, R. A.; Käshammer, J.; Scheumann, V.; Mittler, S. *Chem. Vap. Dep.* **2000**, *6*, 199.

(34) Käshammer, J.; Wohlfart, P.; Weiss, J.; Winter, C.; Fischer, R.; Mittler-Neher, S. *Opt. Mater.* **1998**, *9*, 406.

(35) Busse, S.; Käshammer, J.; Krämer, S.; Mittler, S. *Sens. Actuators, B* **1999**, *60*, 148.

(36) Andres, R. P.; Bein, T.; Dorogi, M.; Feng, S.; Henderson, J. I.; Kubiak, C. P.; Mahoney, W.; Osifchin, R. G.; Reifenberger, R. *Science* **1996**, *272*, 1323.

(37) Brust, M.; Bethell, D.; Kiely, C. J.; Schiffrin, D. J. *Langmuir* **1998**, *14*, 5452.

(38) Weiss, J.; Wohlfart, P.; Winter, C.; Käshammer, J.; Fischer, R.; Mittler-Neher, S. *Adv. Mater. CVD* **1999**, *5*, 165−170.

(39) Thome, J.; Himmelhaus, M.; Zharnikov, M.; Grunze, M. *Langmuir* **1998**, *14*, 17435.

(40) *Römpp Chemielexikon*, 9th edition; Falbe, J., Regitz, M., Eds.; Thieme Verlag: Stuttgart, 1992.

(41) Johannsmann, D. *Macromol. Chem. Phys.* **1999**, *200*, 501.

(42) Aliganga, A. K. A.; Glasser, G.; Lieberwirth, I.; Mittler, S.; in preparation for *Adv. Mater. CVD.*

(43) *CRC Handbook of Chemistry and Physics*, 74th edition; Lide, D. R., Ed.; 1993−1994.

(44) Sauerbrey, G. Z. *Phys.* **1959**, *155*, 206.